Fermi National Accelerator Laboratory

FERMILAB-Pub-76/92-EXP
7200.137

(Submitted to Phys. Rev.)

$\pi^- p$ AT 205 GeV/c: MULTIPLICITIES OF CHARGED AND NEUTRAL PARTICLES; PRODUCTION OF NEUTRAL PARTICLES[*]

D. Ljung,[†] D. Bogert, R. Hanft, F. R. Huson, S. Kahn,
C. Pascaud,[‡] S. Pruss, and W. M. Smart
Fermi National Accelerator Laboratory, Batavia, Illinois 60510

and

H. H. Bingham, D. M. Chew,[§] B. Y. Daugeras,[‡] W. B. Fretter,
G. Goldhaber, W. R. Graves, A. D. Johnson, J. A. Kadyk,
L. Stutte,[||] G. H. Trilling, F. C. Winkelman, and G. P. Yost
Department of Physics and LBL
University of California, Berkeley, California 94720

December 1976

---

[*] Work supported in part by the U. S. Energy Research and Development Administration, the National Science Foundation, and the French Centre National de la Recherche Scientifique.

[†] Present address: Yale University, New Haven, Connecticut 06520.

[‡] Present address: Laboratoire de l'Accélérateur Linéaire, 91 Orsay, France.

[§] On leave from the University of Paris VI, Paris, France.

[||] Present address: California Institute of Technology, Pasadena, California 91109.

I. INTRODUCTION

This paper presents final results on particle multiplicities and characteristics of neutral particle production obtained from an exposure of the Fermilab 30-inch hydrogen bubble chamber to a 205 GeV/c incident π^- beam, with no hybrid system used.[1] Other results from this experiment, including preliminary results on topics discussed here, have been presented elsewhere.[2,3,4,5] Experimental details are discussed in Sec. II; cross sections as a function of charged particle multiplicity and the production of neutral particles are covered in Sec. III.

II. EXPERIMENTAL DETAILS

This section discusses the beam, scanning and measuring, pathlength and density, analysis of two-prong events, corrections for charged multiplicity distributions and event selection and weighting for neutral particles. The corrections to the cross sections and multiplicity distributions are summarized in Table I.

A. Beam

A beam of 10^{11} protons per pulse at 303 GeV/ c was extracted from the Fermilab Synchrotron and targeted one kilometer from the bubble chamber. The secondary beam line to the chamber[2,6] selected negative particles at a production angle of one milliradian and an energy of 205 GeV/c, with a momentum bite of ± 0.1%. At the bubble chamber, the beam extended 6 cm vertically and 2 cm horizontally (FWHM), with an angular divergence of ± 0.25 milliradian.

A differential gas Cerenkov counter measured the K^- and $\bar{p}$ contamination in the unseparated beam to be (1.8 ± 0.2)% and (0.15 ± 0.10)%, respectively, at a point 470 meters upstream of the bubble chamber. From the known π^- and K^- decay properties, the contamination at the chamber is calculated to be (1.4 ± 0.2)% K^- and (0.16 ± 0.10)% $\overline{p}$. These give a net correction for total cross section of (0.0 ± 0.2)%.

The muon contamination was determined by an absorption experiment performed 180 meters upstream of the chamber using one-foot long aluminum and steel blocks. From observation of the fraction of beam reaching the chamber as a function of the number of blocks, the muon contamination at this point, the last bending magnet, was estimated to be (1.0 ± 0.5)%. Adding the contribution of muons from pion decays occurring in the last 180 meters before the chamber raised this number to (2.6 ± 0.5)% at the chamber.[7]

B. Scanning and Measuring

The film was scanned in three views with approximately life-sized projection. The fiducial volume was defined on the scan table, and corresponded in the chamber to a length of approximately 40 cm and a width of 15 cm. About 12 cm of a track was visible before it entered the fiducial volume. For the study of detected neutrals, further fiducial volume criteria were imposed. The primary vertex was required to be in a fiducial volume of length 33.4 cm in the beam direction with an entrance plane 12 cm downstream of the bubble chamber window. The neutral particle vertex was required to be inside a cylinder of radius 22.5 cm and depth 23 cm centered in the chamber. This allowed for a minimum charged track length of 11.5 cm for measurement. This was necessary to resolve ambiguities between gammas and V's. About 31% of the frames were rejected on the grounds that more than 15 tracks entered the fiducial volume, leaving 32,906 frames, with an average of 7 beam tracks per picture.

The information recorded for each event included the number of charged prongs at each (primary or secondary) vertex, and the distance on the scan table to each secondary interaction vertex, V^0 decay point, or γ conversion. Each of the latter two cases was also recorded as G, V, or A according to its identification as a gamma (identified electron or positron), V^0 (having nonzero opening angle or interacting secondary track), or ambiguous (having zero opening angle and no identified electron or positron). In addition, the occurrences of π-μ-e decays, and of positive tracks which could be identified by bubble density as protons, were also noted.

The entire film was scanned twice, with conflicts resolved by a third scan using a special scan table providing a magnification of 3.5X lifesize. The efficiency of the double scan was estimated to be greater than 99% for frames with fewer than 13 beam tracks, not including corrections for short protons. Frames with 13 or more beam tracks were handled separately. Such frames have a relatively high probability of containing more than one event. A downstream event may be obscured by tracks due to the upstream event and either missed or interpreted as a secondary interaction. The existence of such an effect is demonstrated in Fig. 1 and results in a correction of 87 ± 22 events. The loss was found to be independent of multiplicity and was therefore distributed among the multiplicities the same as the observed events.

The overall scanning efficiency correction due to the above effects was 1.3 ± 0.3%. This does not include corrections for missed short protons, which are discussed below.

The G and V scanning efficiencies were greater than 99%. For A's it was found that even after two scans the scan efficiency was 91%. The measuring and fit efficiency for G, V and A was found to be 82%, independent of G, V or A. Further loss of A's and V's close to the vertex is discussed below (E-2).

All G'vs, V's, and A's were measured on image-plane digitizers providing approximately lifesize magnification. The RMS scatter of measured points about the projection on film of the reconstructed trajectory was about 6 μ. GVA's with no successful kinematic fit were remeasured at least once. For the determination of the elastic scattering cross section , all two-prong events were measured on film-plane digitizers with an average RMS scatter of less than 2 μ. A large sample of other topologies was also measured on film-plane digitizers. These measurements were processed by TVGP and SQUAW.

Further details on the scanning and measuring may be found in Reference 8.

C. Pathlength and Density

The total pathlength was determined by counting beam tracks in every tenth picture (and in every picture for 44% of the film) multiplying by the length of the fiducial volume used for charged particle cross sections (39.4 ± 0.2 cm in space), and correcting by -1.74% for pathlength removed by interactions.

This pathlength further was corrected for (1) beam track scanning inefficiency (+0.5 ± 0.5)%; (2) muon contamination at the bubble chamber (-2.6 ± 0.5)%; (3) problems caused by faint tracks which were difficult to see in the picture (0.1 ± 0.1)%; and (4) contamination from events produced by extreme forward-going secondary tracks arising from interactions upstream of the visible region (0.0 ± 0.6)%. The resultant pathlength was found to be $(8.14 \pm 0.10) \times 10^6$ cm. Included in the error estimate is a contribution from the statistical error on the number of beam tracks, estimated to be ± 0.5%.

The hydrogen density was determined from the weighted average range of stopping muons emitted in π^+ decay at rest, and using recent determinations of the mean ionization potential of liquid hydrogen (20.0 eV).[9] The result was (0.0627 ± 0.0005) g/cm^3.

D. Analysis of Two-Prong Events

Of the 1,291 two-prong events found in the scan, 1,189 were successfully measured and reconstructed. Of these 61% had an elastic fit with $\chi^2 < 15$. The resulting differential cross section, $d\sigma/dt$, shown in Fig. 2, is well described by the form Ae^{bt}, for $0.03 < -t < 0.60$ GeV^2. A least-squares fit (solid curve) gives $A = (27.4 \pm 1.7)$ mb/GeV^2 and $b = (8.8 \pm 0.4)$ GeV^{-2}.

These data must be corrected for several effects to obtain the elastic cross section. Firstly, events having protons with $-t < 0.03$ GeV^2 suffer severe scanning losses as seen in Fig. 2. These may be estimated from the exponential fit, under the assumption that the shape of $d\sigma/dt$ undergoes no change in the small t region. For $0.01 < -t < 0.03$, an independent estimate is available, based on the observed distribution of the azimuthal angle of the recoil proton about the beam direction. This requires the assumption that protons emitted close to the plane of the film with $-t > 0.01$ GeV^2 are long enough to be seen. These two estimates are consistent with each other in that t range. The final weighted average result was that 105.5 ± 11 elastic events were lost for $-t < 0.03$ GeV^2.

Secondly, the separation of elastic and inelastic events was studied by several methods. Briefly, these methods consisted of (1) study of those events with observed γ or V^0 which falsely fitted the elastic scattering hypothesis ; (2) removing two tracks from measured four-prong events (or four tracks from measured six prongs, etc.) and subjecting the resulting pseudo-two-prong events to the same kinematic analysis as the real events[8]; (3) simulation of possible background channels by Monte-Carlo techniques[8]; (4) study of the distribution of the component of the transverse momentum imbalance in the plane of the film. All methods gave consistent results within errors. The final weighted average estimate was that 17 ± 5 (2.3 ± 0.7)% inelastic two-prongs were included among the elastics.

Thirdly, a study was performed[8] using simulated measurements of Monte-Carlo events which were processed in the same manner as the real data. It was found that the efficiency with which an elastic event was successfully fitted with $\chi^2 < 15$ was (94.4 ± 1.1)%.

For the 102 (8.5%) events which were unmeasurable, it was possible in most cases to determine the momentum transfer to the proton. The distribution was similar to that for the successfully reconstructed two-prongs. Therefore, these events were apportioned among the elastic and inelastic channels in the same ratio as the events which passed geometry.

To study two-prong inelastic events missed because of a short protor the sample was divided into two classes: beam dissociation and non-beam dissociation. Beam dissociation events were identified[4] as those with squared missing mass recoiling off the proton less than 32 $(\mathrm{GeV}/c^2)^2$. Nc beam dissociation events have a relatively large minimum momentum transfe to the proton, and a visual inspection of their t distribution indicated that short proton losses for these events could be neglected. For the beam dissociation events, the exponential slope of the proton momentum-transfer distribution was fitted as 8.2 ± 0.8 GeV^{-2} for $0.03 < -t < 0.6$ GeV^2. This procedure estimated that 18 ± 3 (4.2 ± 0.6)% events should be added to the two-prong inelastic sample to correct for short protons. The slight error introduced for the beam - dissociation type events due to the fact that the boundary of the kinematical region is at $-t > 0$ was neglected in this calculation.

E. Corrections for Charged Multiplicity Distributions

In order to calculate the distribution of the charged multiplicities, corrections are necessary for those secondary interactions, gamma conversions, and neutral particle decays occurring undetected close to the primary vertex. Corrections are made by extrapolation from the clear region (far from the primary vertex) into the region close to the primary vertex. Further corrections are necessary for Dalitz pair conversions at the origin and for scanning biases against short tracks.

1. Secondary Interactions on Charged Tracks

Figure 3 shows the distribution of projected straight-line distance between primary and secondary vertices, as determined on the scan table. Shown shaded are all events for which the number of secondary prongs could not be resolved, due to confusion with tracks from the primary vertex. Those events are included in the second column of Table II according to the total number of prongs including secondaries. In 90% of the cases, this is an odd number. The solid curve on Fig. 3 shows the predicted distribution based on the total number of outgoing prongs in the experiment, assuming there is one proton for every two events and that all other tracks are pions. Constant total cross sections of 26 mb and 60 mb for πp and pp reactions, respectively, were taken. Contamination from kaons, and corrections for elastic scattering with recoil proton too short to be visible, should not seriously affect the calculation and were neglected.

Based on this curve, an estimated 20 ± 10 secondary interactions were lost at distances less than 2 cm. Further, one observes beyond 10 cm, losses of secondary interactions occurring outside of the fiducial volume. The multiplicity distribution for resolved secondary interactions occurring within 4 cm of the primary vertex is shown in Fig. 4 as the solid line. Most of the unresolved secondary interactions occur in this region. The dashed histogram is constructed proportional to the corresponding distribution for secondary interactions at greater than 4 cm, and is normalized to the total of resolved unresolved, and missed (20 events) secondary interactions estimated to occur within 4 cm. From Fig. 4 it may be seen that there should be 238 total prongs in missed or unresolved secondary interactions within 4 cm of the primary vertex. Scaling this for all distances gives 261 extra prongs due to secondary interactions.

The primary multiplicity distribution was corrected for these tracks by treating four different categories of events: (1) Sixteen events with 3, 5 or 7 tracks. Three of these with a visible secondary vertex were resolved after careful study by a physicist; this subtracts 9 prongs. The remaining 13 events did not have visible secondary vertices. A fit to the proton t-distribution of 4-, 6-, and 8-prong events with identified protons, using a single exponential as before, indicated that 11 ± 3 events of these topologies may have a proton too short to be seen and all of these 13 events were therefore assumed to arise from this source. (2) Sixty-three odd-prong events with greater than 7 tracks and a visible but unresolved secondary interaction. From the distribution in Fig. 4 the average multiplicity of secondary interactions is 4. Therefore it is assumed these events are primary events with one secondary having a 4-prong secondary event and thus 3 prongs were subtracted from each one. This subtracted 189 prongs.

(3) Seven even-prong events with a visible but unresolved secondary interaction. It was assumed that these had a secondary interaction with a lost track and therefore two prongs were subtracted for each. This corresponds to 14 prongs subtracted. (4) Twenty even-prong events with missed secondary interactions. Since these events are unidentified it was assumed that their distribution was the same as the 63 events in (2) above. As in (3) above, two prongs were subtracted for each. This corresponds to 40 prongs subtracted.

This method of correction subtracts a total of 252 prongs, consistent with the 261 estimated above.

2. Missed GVA's

Figures 5a and 5b show the distribution of scan table distances between the primary vertex and identified G or A vertex for G's and A's which fit $\gamma + p \rightarrow e^{+}+e^{-}+p$.[10] From the kinematic fits, it was discovered that virtually all identified G's were γ conversions. Likewise, most identified V's fitted to K^{0}, Λ, or $\bar{\Lambda}$ decays, as expected.

The dashed curve of Fig. 5a has a slope determined by the conversion length (12.7 m at large γ energies) and has been normalized to the number of conversions observed from 4 to 12 cm. Beyond 12 cm there are losses due to fiducial volume restrictions. The curve in Fig. 5a is compatible with the data for all distances less than 12 cm, suggesting that within that distance losses of $\gamma \rightarrow e^{+}e^{-}$ events classified as G are small, even close to the primary vertex.[11]

Figure 5b indicates a severe loss of A's within 8 cm of the primary vertex for the component fitting to γ's. The fitting procedures and event selection will be discussed below. The curve in Fig. 5b is calculated as in Fig. 5a, but normalized in the range 8 cm to 12 cm. This gives 90 ± 15 A's missed in scanning that were gammas converting inside the fiducial volume after corrections for scanning and measuring efficiency.

Figure 6a and 6b present the same data as Fig. 5 plus including potential length information. The variable Q_γ is defined by

$$Q_\gamma \equiv \frac{\int_o^x \exp[-x/x_o]\, dx}{\int_o^{x_p} \exp[-x/x_o]\,dx}$$

x = distance to gamma conversion
where x_o = conversion length (12.7 m)
x_p = potential conversion length.

This confirms the loss of 90 ± 15 A's at small x and shows no evidence for further loss of gammas.

Figure 6c and 6d show the corresponding figures for neutral strange particles (V). Here Q_V is defined by

$$Q_V \equiv \frac{\int_o^x \exp\ [-x/\lambda]dx}{\int_o^{x_p} \exp\ [-x/\lambda]dx}$$

x = distance to V decay
where $\lambda = c\gamma\beta T$ = mean decay distance
x_p = potential decay length.

Here it is clear that strange particles are lost both when identified (36 ± 10) and unidentified (10 ± 5). This gives 58 ± 15 neutral strange particles missed after corrections for scanning and measuring efficiencies.

The multiplicity distribution was corrected by assuming the missed A's and V's were distributed among the topologies in the same proportions as the distributions of A's and V's actually found.

3. Dalitz Pairs

During the scan, 123 Dalitz pairs were identified using a curling electron or positron as the signature and were included in the primary multiplicity. Under the assumption that all produced γ's arise from π^0 decay, the number of π^0's, and hence, the number of Dalitz pairs, can be estimated. From 51,200 weighted γ's, 299 Dalitz pairs are expected. Thus an estimated 176 Dalitz pairs were not indentified. On the grounds that these events contain an energetic e^+e^- pair, it was assumed that they were distributed among the multiplicities in the same manner as the A's, 80% of which are γ conversions containing energetic e^+e^- pairs.

F. Event Selection and Weighting for Neutral Particles

Out of a total of 1,644 detected neutrals noted in the scanning, 31% fell outside of the restricted fiducial volume used in the neutrals study (Sec, III-C,D,E). Physicists further rejected a total of 3.6% because they did not point to an event or were not genuine G, V, or A candidates. The remaining 1,068 were processed through TVGP and SQUAW. Kinematic fits (3c) to $\gamma(+p) \rightarrow e^-e^+ (p)$,[10] $K^0_S \rightarrow \pi^-\pi^+$, $\Lambda \rightarrow \pi^-p$, and $\overline{\Lambda} \rightarrow \overline{p}\pi^+$ were attempted assuming a line of flight from the presumed (primary) origin.

Acceptable fits were required to have a χ^2 less than 20. The transverse momentum of each of the outgoing tracks was, in addition, required to be less than 15 MeV/c for γ fits, and greater than 15 MeV/c for neutral decay fits. This cut was used to obtain the proper known distributions for Fig. 7. Even without this cut 13 of the $\bar{\Lambda}$ (all except one, backward in the center of mass) were unambiguously identified as a V

There remained 119 successfully reconstructed events with no acceptable fit, 815 events with exactly one acceptable fit, and 61 events with two fits. In the latter category there were 41 K_s^o -Λ ambiguities, 19 K_s^o -$\bar{\Lambda}$ ambiguities, and one γ-$\bar{\Lambda}$ ambiguity. Because of the high momentum of most of the tracks, ionization information was not useful in resolving the majority of these ambiguities and each event has been assigned to the fit with the lowest χ^2. In more than half the cases, the two χ^2 differ by a factor of two or more. Figure 7 gives the fitted transverse momentum distributions for the various neutral strange particles as chosen in this manner. These distributions are as expected $\frac{p_\perp}{q^2\sqrt{1-p_\perp^2/q^2}}$ where q is the maximum p .

The cosine of the polar decay angle (θ_D) of the emitted negative, in the rest system of the neutral, is displayed in Fig. 8. The distribution of the 60 K_s^o/Λ and $K_s^o/\bar{\Lambda}$ events are shown as shaded. The distribution of the unambiguous events, 204 K_s^o, 83 Λ, and 13 $\bar{\Lambda}$, is shown unshaded. The one γ-$\bar{\Lambda}$ ambiguous event has been called a $\bar{\Lambda}$.

These distributions are expected to be flat in the absence of biases and significant longitudinal polarization. The ambiguous events assigned here to Λ would tend to fall at cos $\theta_D \simeq -1$ if assigned to K_s^o, seriously distorting the decay angular distribution of the latter, if done in significant number. Assignment of a significant number of the ambiguous events here classified as $\bar{\Lambda}$ to the K_S^o channel would seriously distort the $\bar{\Lambda}$ distribution. There is no evidence in these plots for a statistically significant depletion (or enhancement) near $\cos\theta_D = \pm 1$, where losses (or gains) due to γ mis-identification would be expected to occur.

An additional investigation of the K/Λ and $K/\bar{\Lambda}$ ambiguities was made by requiring $|\cos\theta_D| < 0.85$ for accepted K^o fits, $\cos\theta_D > 0$ for Λ fits, and $\cos\theta_D < 0$ for $\bar{\Lambda}$ fits. Only two ambiguous events remained. The cross sections and all of the distributions to be discussed below remained the same (within ± 1 standard deviation) as those found using the assignments according to the lowest χ^2.

The ambiguous events (including the one γ-$\bar{\Lambda}$ ambiguity) have therefore been assigned according to the best χ^2. Under the assumption that 1/4 of the cases in which the χ^2 differed by more than a factor of two and 1/3 of the rest are incorrectly assigned, an estimate of contamination can be obtained. The estimated contamination in the K_S^o sample of Λ or $\bar{\Lambda}$ is 4%; the K_S^o contamination in the Λ and $\bar{\Lambda}$ samples is estimated at 8% and 12%, respectively.

Independent weighting factors used in the cross-section calculation correct for (a) the decay or conversion probability (including unseen decay modes); (b) unmeasurable events; i.e., those not successfully measured or fitted; and (c) scanning efficiency.

As demonstrated above, losses of events classified as G at close distances from the production vertex appear to be small because of their striking appearance. The minimum detectable neutral length was therefore taken to be zero, and a separate correction was made for A and V type events.[12] The decay or conversion probability was therefore determined solely by the projected range to the edge of the fiducial cylinder (see Sec. II-B), the type of particle, and its reconstructed momentum. For γ conversions, the pair production cross sections given by Knasel[13] were used.

Corrections to the cross sections for unmeasurable events were done separately for those classified as G, V, or A. These corrections were applied as a function of the charged multiplicity of the event.

The correction for A's and V's close to the primary vertex, missed by the scanners, was in the form of a weighting factor, and was applied only to those found in the scan at distances less than 8 cm (Fig. 6). This procedure was checked for all events (80% of the A's are identified as γ's after measurement), by reanalyzing the data with a minimum length requirement of 8 cm imposed, and adjusting the weights accordingly. No significant difference was found in any of the distributions by using this second method. Therefore it was concluded that possible errors introduced by this procedure could be neglected.

The average weight per event was: 89.6 for γ, 3.59 for K_s^o, 3.56 for Λ, and 5.83 for $\overline{\Lambda}$. Because of the large momenta involved, K_s^o, Λ, and $\overline{\Lambda}$ produced forward in the center of mass have poor detection efficiency, and correspondingly large weights. In fact Λ and K_s^o are only detected up to an x $\left(x \equiv \frac{2p_L^{c.m.}}{\sqrt{s}}\right)$ of 0.3 and $\overline{\Lambda}$ to 0.1.

G. Missing Mass and Momentum Measurements

The sum of the neutrals recoiling against the charged particles may be studied by the missing mass technique. For this study, events with 4C fits (i.e., no missing neutrals) are removed. Further, events having vertices downstream of the chamber center are excluded, so that charged tracks have at least 30 cm of potential measurable length. All charged tracks are taken to be pions, unless an identified proton is preser

The expected errors in the missing mass (m_o) and momentum (p_o) are strong functions of the missing momentum (Fig. 9a, b) and multiplicity. At $p_o > 150$ GeV, the measurements of the (slow) charged tracks are sufficiently precise that the expected error in m_o averages around one GeV, and in p_o around 15 GeV/c or less. As the multiplicity increases, the average error tends to decrease, so that in the 10-prong events, the errors are only ~10% of those for 2-prong events.

If high-momentum charged tracks are present, the errors may be sufficiently large that p_o may be negative. In this case, it follows from simple kinematical considerations that p_o^2 will usually exceed E_o^2, the square of the missing energy. Then m_o^2 will be negative. From inspection of the events fitting elastic scattering, the most extreme case of this effect, it has been verified that both p_o and m_o^2 are symmetric about a mean ~0, so that large measurement uncertainties do not imply measuring biases.

III. RESULTS

The results for cross sections, multiplicities and neutral particle production are presented in this section. Table II presents the topological cross sections.

A. Cross Sections

The total cross section was determined to be (24.19 ± 0.44) mb, in good agreement with the result of Carroll et al.,[14] (24.28 ± 0.06) mb.

The elastic cross section was computed to be 3.18 ± 0.13 mb. The energy dependence of this cross section is shown in Fig. 10. The data were taken from reference 15, 16, and 17.

The least squares fit of the elastic scatter events to Ae^{bt} for $0.03 < -t < 0.60$ GeV^2 gives $A = (27.4 \pm 1.7)$ mb/GeV^2 and $b = (8.8 \pm 0.4)$ GeV^{-2} (see Fig. 2). This is consistent with an optical theorem calculation assuming a purely imaginary amplitude in the forward direction and using the Caroll et al.[14] cross section, which yields:

$$\left.\frac{d\sigma}{dt}\right|_{t=0} = 30.1 \pm 0.1\ \mathrm{mb/GeV^2}.$$

B. Charged Particle Multiplicities

The third column of Table II gives the estimated number of events after all corrections are applied, and column 4 gives the corresponding cross sections. Figure 11 shows the topological cross sections for $\pi^- p$ vs p_{lab}. Figure 12a shows the average multiplicity for $\pi^- p$ and pp interactions for 100 GeV/c and above as a function of the energy or Q $(\sqrt{s} - m_{beam} - m_{target})$ in the center of mass. The Q is used rather than $\sqrt{s}$ since that makes π^- and p average multiplicities fall on the same line, $\bar{n}_{ch} = a + b\ \ln Q$.

As pointed out by J. Erwin et al.[18] one might expect the multiplicity distribution to fit a Poisson distribution[19] in produced pairs $n_p = \frac{n_{ch}}{2} - 1$

$$\sigma_{n_p} = \frac{\sigma_o e^{-\bar{n}_p} \left(\bar{n}_p\right)^{n_p}}{n_p!}$$

If this is true then a plot of log $(n_p! \sigma_{n_p})$ vs n_p will be a straight line with a slope of log $\bar{n}_p$. Such a plot is shown in Fig. 13. The straight line fits are made to $n_p \geq 3$. $[\bar{n}_p$ (for $n_p \geq 3) \equiv \bar{n}_{p3}]$. The deviation from a straight line for $n_p < 3$ can be explained as additional events due to diffraction dissociation (two component theory for the multiplicity distribution[20]). Similar fits to other pion and proton data[21] give the values of $\bar{n}_{p3}$ plotted in Fig. 12b. Note $\bar{n}_{p3}$ (Fig. 12b) is a linear function of log Q and the same for pions and protons.

C. Neutral Pion Production

By assuming that all gammas come from π^0 decay, some characteristics of neutral pion production can be determined. Figure 14 gives the average number of π^0's produced as a function of the charged multiplicity. The number of π^0's is consistent with a linear increase as a function of n_{ch} and about equal to the number of outgoing negative (or positive) charges.

To study the momentum distributions for the gammas, the charged pions were taken to be π^0's and allowed to "decay" (isotropically) into (Monte Carlo) giving corresponding gamma distributions. Figure 15 compares the parallel and perpendicular momentum distributions showing that the π^0's (real γ) have the same distributions as the π^+ (that is fake $\pi^+ \to 2\gamma$). There were no γ's observed above 80 GeV/c in the laboratory system and above $p_\perp$ of 1.1 GeV. It is believed these few expected gammas were lost in the geometry program.

D. Cross-Section Results for Neutral Strange Particles

Tables III, IV and V give the number of fitted neutrals, the weighted number of neutrals, the cross sections, and the average number of neutrals per inelastic collision, as a function of n_{ch} (the number of charged particles) for K_s^0's, Λ's, and $\bar{\Lambda}$'s, respectively. No attempt has been made to resolve the Λ/Σ^0 ambiguity. Inclusive results are also given for neutrals produced forward or backward in the center of mass. These results apply to the kinematic region $x < 0.3$ for K_s^0 and Λ production and $x < 0.1$ for $\bar{\Lambda}$ production due to the small detection efficiency in the forward region. An estimat of the possible error involved in determining the inclusive total cross sections can be determined from the facts that detecting one additional event at $x = 0.3$ adds approximately 0.15 mb to the cross section while detecting one at $x = 1.0$ adds 0.5 mb.

Figure 16 compares the neutral inclusive cross sections in this experiment with other π^-p data.[22,23,24] The K_s^0 and $\bar{\Lambda}$ cross sections are rising with increased energy. However, the Λ cross section seems to be leveling off above 40 GeV/c. This constant cross section is consistent with interpreting most of Λ production as being associated with the proton vertex. Similar behavior of neutral strange particle inclusive cross sections is observed in pp interactions.[25]

Figure 17 shows the average number of neutral strange particles produced per inelastic interaction as a function of n_{ch}. The Λ and K_s^0 figures also show 100 GeV/c π^-p data[23] for comparison. Within the rather large uncertainties of the present data there appears to be no strong correlation between neutral strange particle production and n_{ch} (ignoring the special case of $n_{ch} = 0$). It appears that the probability of making a neutral strange particle is independent of the charged multiplicity. This behavior is to be contrasted with the strong linear correlation found between π^0 production and n_{ch}. The lack of a strong correlation between neutral strange particle production and n_{ch} is observed in pp interactions for n_{ch} greater than four.[25] Kaiser[26] predicts that the average number of neutral particles produced should be linearly related to n_{ch}. His model applies equally to π^0 and neutral strange particle production, although the exact correlation depends on the particle produced. The lack of a strong correlation in neutral strange particle production probably casts doubt on his model.

If the data can be factorized into a forward (in the center of mass) part associated with the beam and backward part associated with the target, then the present data on K_s^o, Λ, and $\bar{\Lambda}$, for $x < 0$, may be compared with pp data[25] at the same energy. Table VI, which gives the average number of backwards neutrals produced per inelastic collision, shows that the results of this experiment agree very well with the 205 GeV/c pp experiment.

E. Momentum Dependence of Neutral Strange Particle Production

The dependence of the neutral particle inclusive cross sections on the Feynman scaling variable x is shown in Fig. 18, for K_s^o, Λ, and $\bar{\Lambda}$, respectively. These figures plot $F_1(x)$ as a function of x.

$$F_1(x) = \int \frac{2E_{c.m.}}{\pi\sqrt{s}} \frac{d^2\sigma}{dxdp_\perp{}^2} dp_\perp{}^2 .$$

The K_s^o and Λ figures also show corresponding results from pp interactions at 205 GeV/c.[25] For this comparison these data have been scaled by the factor $\sigma_{inelastic}(\pi^- p)/\sigma_{inelastic}(pp) = 0.65$. Good agreement is observed between the $\pi^- p$ and pp distributions. Agreement in the backward direction is further evidence for factorization. The pp and $\pi^- p$ data show reasonable agreement in the limited region accessible to the present experiment in the forward direction.

These distributions have also been compared with the corresponding data for γ, K_s^o, and Λ production in $\pi^- p$ interactions at 100 GeV/c[22] (not shown). Within the errors, there is agreement between the experiments in all cases, consistent with scaling. This is, in addition, a test for the hypothesis of limiting fragmentation,[27] which appears to be consistent with the data within the errors.

It appears from Fig. 18 and Table IV that Λ production is much larger in the backward direction than in the forward, indicating that it may be primarily associated with target fragmentation consistent with the conclusion of the previous section. In contrast, the $\bar{\Lambda}$ production appears to concentrate in the central region. Note that the Λ and $\bar{\Lambda}$ cross sections are approximately equal at $x = 0$.

There are three events which have an observed $\Lambda\bar{\Lambda}$ pair. The values of x for these are $(\Lambda,\bar{\Lambda}) = (-0.10, -0.01)$; $(-0.10, -0.03)$; and $(-0.62, -0.53)$. For all three observed pairs, the difference in x between the particles is 0.09 or less, even though the range of x over which these particles are observed singly is an order of magnitude larger. The $\Lambda\bar{\Lambda}$ mass is correspondingly near threshold for these pairs (less than 2.5 GeV/c^2). This is consistent with a model in which the $\bar{\Lambda}$ comes from a mesonic state decaying into $\Lambda\bar{\Lambda}$, $\bar{K}^0\bar{\Lambda}p$, etc, and produced primarily in the central region.

Table VII compares the mean multiplicity dependence of Λ and $\bar{\Lambda}$ production near the central region $(x > -0.15)$ with dependence away from the central region. The first two moments of the distribution of n_{ch} are more than two standard deviations greater for central-region Λ production than for the backward production. This may indicate a different production mechanism for central-region Λ events, in support of the hypothesis that Λ production in that region is frequently associated with a $\bar{\Lambda}$.

Table VIII contains a summary of all observed cases of multiple neutral strange particle production, with associated cross sections.

Figure 19 shows F_2 (p_T^2) as a function of p_T^2 for the neutral strange particles.

$$F_2(p_\perp{}^2) = \int \frac{2E_{c.m.}}{\pi\sqrt{s}} \frac{d^2\sigma}{dx dp_\perp{}^2} dx.$$

The solid lines are fits to the data of the form A exp $(-bp_T^2)$. The results of the fits are shown in Table IX. The strange particles appear to have similar slopes. For $\pi^- p$ at 40 GeV/c,[22] the corresponding slopes for K_s^0 and Λ production are 4.53 ± 0.54 $(\mathrm{GeV/c})^{-2}$ and 4.71 ± 0.92 $(\mathrm{GeV/c})^{-2}$, respectively. Thus, those two types of strange particles appear to have similar slopes, the magnitude of which is not a strong function of incident energy. For pp reactions at 205 GeV/c,[25] the K_s^0 and Λ distributions are found to have slopes of 4.6 ± 0.8 $(\mathrm{GeV/c})^{-2}$ and 2.8 ± 0.8 $(\mathrm{GeV/c})^{-2}$, respectively. In both cases, these slopes are consistent with the results of the present experiment.

F. Sum of all Neutrals

The average missing momentum (p_0) is displayed in Fig. 20 as a function of the number of charged tracks (n_{ch}) averaged over all events of that topology. Events identified by kinematics as having no neutrals (i.e. 4c fits) have been removed. It may be seen that the average momentum carried off by the sum of all neutrals is remarkably constant, equal to about 1/3 of the total available momentum. This is consistent with the observation, which was based on γ conversions, that most of the neutrals are π^0's and that $\bar{n}_{\pi^0}$ is a nearly constant fraction (~1/3) of the total number of pions for the bulk of the multiplicity distribution $(n_{ch} \leq 16)$.

For comparison, Fig. 20 also displays the corresponding average vector summed momenta for the positive (p_+) and the negative (p_-) tracks. Multiplicity dependence is apparent for the charged tracks.

Furthermore, the negatives have significantly more momentum than the positives. This is perhaps most naturally interpreted as a leading particle effect.[28] It is interesting to note that this evidence for leading particle effects is present even in the highest multiplicities shown.

IV. CONCLUSIONS

The general conclusion of this experiment is that there are many similarities between the π^-p and pp interactions. The average charged multiplicity for π^-p and pp are consistent with log Q dependence for momenta greater than 100 GeV/c. The multiplicity distributions can be interpreted as being made up of two components: a diffraction dissociation component associated with lower multiplicity and cluster production component (Poisson distribution in produced pairs) associated with higher multiplicity. The average number of pairs produced, assuming a Poisson distribution, also is consistent with log Q dependence.

The strange-particle production is similar for π^-p and pp after normalization of pp cross sections by multiplying by $\sigma_{\pi p}^{\text{inel.}} / \sigma_{pp}^{\text{inel.}}$. The primary Λ production is associated with the proton vertex, and is approximately constant as a function of energy. The $\bar{\Lambda}$ and K_s^0 are principally produced in the central region in the center of mass consistent with particle-antiparticle production. Both $\bar{\Lambda}$ and K_s^0 inclusive cross sections are increasing with incident particle energy.

The π^0 production is as expected, i.e. equal to approximately π^+ in number and in longitudinal and transverse momentum distribution. Also approximately 1/3 of the energy for the topology goes into neutrals, in contrast to the strong topology dependence seen for the energy of the positive and negative tracks.

REFERENCES

1. One of the hybrid systems was in operation, but was not used for the present results.
2. D. Bogert et al., $\pi^- p$ Interactions at 200 GeV/c, AIP Conference Proceedings No. 12, p. 60 (Vanderbilt Conference - 1973). See also, D. Bogert et al., Phys. Rev. Letters 31, 1271 (1973).
3. D. Bogert et al., Inclusive γ, K_s^o, Λ^o and $\overline{\Lambda}^o$ Production by 205 GeV/c $\pi^- p$ Interactions (submitted to Berkeley Meeting of the American Physical Society, 1973). See also D. Bogert et al., Inclusive γ, K_s^o, Λ^o and $\overline{\Lambda}^o$ Production in 205 GeV/c $\pi^- p$ Interactions (submitted to the XVIIth International Conference on High-Energy Physics, London (1974).
4. F. C. Winkelmann et al., Phys. Rev. Letters 32, 121 (1974).
5. H. H. Bingham et al., Phys. Letters 51B, 397 (1974).
6. For a description of this beam line, see, for example, J. Lach and S. Pruss, Hadron Beams in the Neutrino Area, TM-285 (1971), and Instrumentation of the Hadron Beams in the Neutrino Area, TM-298 (1971).
7. We wish to thank R. L. Lander and J. Klems for helpful comments on this analysis. See J. Klems, NAL-48 Internal Memo on Contamination of the Beam (University of California, Davis, 1973). The muon contamination at the chamber was incorrectly reported as (2.2 ± 0.3)% in Reference 2.
8. Linda Gail Stutte, Two- and Four-Prong Interactions in $\pi^- p$ at 205 GeV/c, (Ph.D. Thesis), Particle Physics Group, University of California, Berkeley (1974).
9. J. Kadyk and G. Yost, Lawrence Berkeley Laboratory, Trilling-Goldhaber group internal memo TG-191 (1973).

10. The recoil proton for the gamma conversions was treated in the fit as though it had a "measured" momentum of 0 ± 2 MeV/c.
11. A separate correction to the event multiplicity introduced for missed Dalitz pairs will largely remove any errors introduced by mis-identification of a Dalitz pair as a G.
12. Errors introduced through mis-classification of Dalitz pairs or other tracks as G or V will be neglected. It was assumed that any such events will not be successfully measured and reconstructed, and therefore no bias will occur in distributions based upon measured quantities.
13. T. M. Knasel, DESY Reports Nos. 70/2 and 70/3, 1970 (unpublished).
14. A. S. Carroll et al., Phys. Rev. Letters 33, 932 (1974).
15. Data below 20 GeV/c from K. J. Foley et al., Phys. Rev. Letters 11, 425 (1963).
16. Data 30-55 GeV/c from A. P. Bugorsky et al., Studying Elastic Scattering of Negative Pions on Protons at Small Angles in Momentum Range 30-55 GeV/c, Institute for High Energy Physics (paper submitted to XVIth International Conference on High Energy Physics, Batavia, USA, 1972).
17. For 50 to 200 GeV, Fermilab Single Arm Spectrometer Group, 35, 1195 (1975); C. W. Akerlof Phys. Rev. Lett. 35, 1406 (1975).
18. J. Erwin et al., Phy. Rev. Lett 32, 254 (1974).
19. For example, C. P. Wang, Phy. Rev. 180, 1463 (1969); C. DeTar, Phys. Rev. D3, 128 (1971).

20. C. Quigg and J. D. Jackson, Fermilab Publication NAL-THY-93. W. R. Frazer, R. D. Peccei, S. S. Pinsky, and C. I. Tan, Phys. Rev. D7, 2647 (1973); J. Lach and E. Malamud, Phys. Lett. 44B, 474 (1973).

21. 100 GeV π^-p E. L. Berger et al., Nuc. Phys. B77, 365 (1974).
147 GeV π^-p D. G. Fong et al., Phys. Lett. 53B, 290 (1974).
250 GeV π^-p S. Hagopian et al., "Topological Cross Sections for π^-p Interactions at 250 GeV/c." Florida State University preprint.
100 GeV pp See Reference 19 and C. Bromberg et al., Phys. Rev. Lett. 31, 1563 (1973).
205 GeV pp G. Charlton et al., Phys. Rev. Lett. 29, 575 (1972).
303 GeV pp F. T. Dao et al., Phys. Rev. Lett. 29, 1627 (1972).
400 GeV pp C. Bromberg et al., ibid.

22. P. H. Stuntebeck et al., Phys. Rev. D9, 608 (1973) discuss 18.5 GeV/c π^-p interactions.
Bucharest et al., collaboration, "Neutral Strange Particle Production in π^-p, π^-n, and π^-c Interactions at 40 GeV/c" Bucharest report September 1973.

23. E. L. Berger et al., "Production of K_s^o, Λ and γ in 100 GeV/c π^-p Interactions," CERN/D.Ph.II/PHYS 74-27, submitted to the XVIIth International Conference on High-Energy Physics, London, (1974).

24. D. Bogert et al., "Neutral Strange Particle Production in π^-p Interactions at 250 GeV/c", Fermilab report submitted to Seattle Meeting, August 1975.

25. K. Jaeger et al., "Production of Strange Particles and of γ-Rays in Proton-Proton Interactions at 205 GeV/c", submitted to Berkeley Meeting of the American Physical Society, 1973. For the purposes of Table VII, their Λ and $\bar{\Lambda}$ results have been divided by two to restrict the result to the backward hemisphere. Their K^o result has been divided by four because they included K_L^o in their calculation. See also G. Charlton et al., Phys. Rev. Lett. 30, 544 (1973).

26. G. D. Kaiser, "The Use of the Approximately Normal Distribution to Describe the Production of Neutral Particles," Daresbury Preprint DNPL/P170 July 1973.

27. J. Benecke, T. T. Chou, C. N. Yang, and E. Yen, Phys. Rev. 188, 2159 (1969).

28. G. Y. Yost et al., "Leading Particles in π^-p Interactions at 205 GeV/c," submitted for publication (1975).

TABLE I

Corrections for Cross Sections and Multiplicities

Cross Sections:

Correction	
μ^- in beam	+2.6 ± 0.5%
K^-, $\bar{p}$ in beam	+0.0 ± 0.2%
Scan efficiency	+1.3 ± 0.3% to all events
Early beam	-0.1 ± 0.1%
Non beam	+0.0 ± 0.6%
Beam scan efficiency	-0.5 ± 0.5%
Short proton loss ($-t < 0.03$ GeV^2)	+14.4 ± 0.8% to elastics
Inelastic background	-2.3 ± 0.7% to elastics
Kinematic fitting inefficiency	+5.6 ± 1.1% to elastics
Measurement efficiency	+8.5% to two-prong events
Short proton loss ($-t < 0.03$ GeV^2)	+4.2 ± 0.6% to inelastic two-prongs

Charged Particle Multiplicity:

Corrections	No. Prongs Added	Correction To $\bar{n}$
Missed and unresolved secondaries	-252	-0.041
Missed protons $\geq$ 4 prongs	+13	+0.002
Missed protons inelastic two prongs	+36	+0.006
Missed G < 8 cm	+0	+0
Missed V < 8 cm	-90	-0.014
Missed A < 8 cm	-206	-0.032
Dalitz pairs	-352	-0.056
		Net -0.135

TABLE II

Topological Cross Sections in 205 GeV/c $\pi^- p$ Interactions

Number of Prongs		Events Found	Corrected Number[a]	Cross Section (mb)[b]
0		3	$3^{+5}_{-2.5}$	$0.010^{+0.016}_{-0.008}$
1		0		
2	Total	1291	1476 ± 38	4.86 ± 0.14
	Elastic		966 ± 34	3.18 ± 0.13
	Inelastic		510 ± 26	1.68 ± 0.09
3		6		
4		1020	1072 ± 35	3.53 ± 0.13
5		6		
6		1137	1195 ± 37	3.93 ± 0.13
7		4		
8		1219	1259 ± 38	4.14 ± 0.14
9		6		
10		1003	1013 ± 35	3.33 ± 0.12
11		14		
12		665	673 ± 30	2.21 ± 0.10
13		11		
14		361	341 ± 23	1.12 ± 0.08
15		9		
16		192	189 ± 17	0.62 ± 0.06
17		10		
18		98	94 ± 12	0.31 ± 0.04
19		6		
20		36	29 ± 8	0.10 ± 0.03
21		4		
22		11	8 ± 5	0.026 ± 0.016
23		3		
24		2	$1^{+3}_{-0.5}$	$0.003^{+0.010}_{-0.002}$
25		0		
26		0	0^{+2}_{-0}	$0.0^{+0.007}_{-0.0}$
27		0		
28		1	$1^{+2}_{-0.5}$	$0.003^{+0.007}_{-0.002}$
TOTAL		7118	7354 ± 88	24.19 ± 0.44

---

[a] Total error is the statistical error combined with the error on the corrections.

[b] The cross section errors also include errors due to the determination of the total pion path length and the hydrogen density.

TABLE III-A

Cross Sections for $\pi^- p \rightarrow K_s^0$ + Anything

for x<0.3

Number of Charged Particles Produced n_{ch}	Number of Fitted K_s^0	Weighted Number	σn_{ch} (K_s^0) mb	$\bar{n}_{K_s^0}$ per inelastic interaction
0	1	2.1	$0.008 \begin{smallmatrix} + 0.041 \\ - 0.004 \end{smallmatrix}$	$0.82 \begin{smallmatrix} + 4.10 \\ - 0.41 \end{smallmatrix}$
2	8	135.5	0.53 ± 0.45	0.317 ± 0.27
4	35	148.0	0.58 ± 0.15	0.165 ± 0.04
6	48	148.5	0.58 ± 0.12	0.148 ± 0.03
8	39	121.8	0.48 ± 0.12	0.115 ± 0.03
10	56	156.5	0.62 ± 0.12	0.184 ± 0.04
12	33	120.2	0.47 ± 0.1	0.214 ± 0.05
14	10	27.8	0.11 ± 0.04	0.097 ± 0.04
16	11	38.0	0.15 ± 0.05	0.240 ± 0.08
18	7	29.2	0.11 ± 0.05	0.371 ± 0.17
Total	248	427.6	3.64 ± 0.61	0.173 ± 0.029
Forward*	54	439.3	1.72 ± 0.51	0.082 ± 0.024
Backward	194	488.3	1.92 ± 0.24	0.091 ± 0.011

*For 0<x<0.3

TABLE III-B

Cross Sections for $\pi^- p \rightarrow K_s^0$ + Anything

for $x<0.0$

Number of Charged Particles Produced n_{ch}	Number of Fitted K_s^0	Weighted Number	σn_{ch} (K_s^0) mb	$\bar{n}_{K_s^0}$ per inelastic interaction
0	0	0	0	0 0
2	7	18.2	0.071 ± 0.03	0.042 ± 0.02
4	27	75.6	0.30 ± 0.06	0.084 ± 0.02
6	39	104.8	0.41 ± 0.07	0.105 ± 0.02
8	31	66.1	0.26 ± 0.05	0.063 ± 0.01
10	45	103.6	0.41 ± 0.06	0.122 ± 0.02
12	25	70.5	0.28 ± 0.06	0.125 ± 0.03
14	8	16.7	0.066 ± 0.03	0.059 ± 0.03
16	8	23.9	0.094 ± 0.04	0.152 ± 0.07
18	4	8.9	0.035 ± 0.02	0.113 ± 0.07
Backward	194	488.3	1.92 ± 0.24	0.091 ± 0.011

TABLE IV-A

Cross Sections for $\pi^- p \to \Lambda$ + Anything for $x<0.3$

Number of Charged Particles Produced n_{ch}	Number of Fitted Λ	Weighted Number	$\sigma_{n_{ch}}(\Lambda)$ mb	$\bar{n}_{\Lambda^o}$ per inelastic interaction
2	16	86.1	0.34 ± 0.16	0.204 ± 0.094
4	22	56.8	0.22 ± 0.06	0.063 ± 0.016
6	22	62.6	0.25 ± 0.07	0.063 ± 0.018
8	23	82.6	0.32 ± 0.11	0.078 ± 0.027
10	21	80.0	0.32 ± 0.10	0.095 ± 0.030
12	9	51.6	0.20 ± 0.09	0.092 ± 0.040
14	3	12.5	0.05 ± 0.03	0.044 ± 0.028
16	1	1.3	$0.005^{+0.026}_{-0.003}$	$0.008^{+0.041}_{-0.004}$
18	1	1.2	$0.005^{+0.002}_{-0.002}$	$0.015^{+0.069}_{-0.007}$
Total	118	434.7	1.71 ± 0.34	0.081 ± 0.016
Forward*	7	119.2	0.47 ± 0.21	0.022 ± 0.010
Backward	111	315.5	1.24 ± 0.22	0.059 ± 0.011

*For $0<x<0.3$

TABLE IV-B

Cross Sections for $\pi^- p \rightarrow \Lambda$ + Anything

for $x<0.0$

Number of Charged Particles Produced n_{ch}	Number of Fitted Λ	Weighted Number	$\sigma_{n_{ch}}$ (Λ) mb	$\bar{n}_{\Lambda^o}$ per inelastic interaction
2	14	33.5	0.13 ± 0.04	0.078 ± 0.021
4	22	56.3	0.22 ± 0.06	0.063 ± 0.016
6	22	62.6	0.25 ± 0.07	0.063 ± 0.018
8	22	59.0	0.23 ± 0.06	0.056 ± 0.016
10	19	59.9	0.23 ± 0.06	0.071 ± 0.017
12	8	36.7	0.14 ± 0.06	0.065 ± 0.03
14	2	5.0	0.02 ± 0.02	0.02 ± 0.02
16	1	1.3	$0.005 {}^{+0.026}_{-0.003}$	$0.008 {}^{+0.041}_{-0.004}$
18	1	1.2	$0.005 {}^{+0.002}_{-0.002}$	$0.015 {}^{+0.069}_{-0.007}$
Backward	111	315.5	1.24 ± 0.22	0.059 ± 0.011

TABLE V-A

Cross Sections for $\pi^- p \rightarrow \bar{\Lambda}$ + Anything for $x<0.1$

Number of Charged Particles Produced n_{ch}	Number of Fitted $\bar{\Lambda}$	Weighted Number	$\sigma_{n_{ch}}(\bar{\Lambda})$ mb	$\bar{n}_{\bar{\Lambda}^o}$ per inelastic interaction
2	1	16.4	$0.06 \, {}^{+0.06}_{-0.04}$	$0.038 \, {}^{+0.038}_{-0.025}$
4	3	16.2	0.06 ± 0.04	0.017 ± 0.011
6	8	39.5	0.15 ± 0.08	0.038 ± 0.020
8	5	25.6	0.10 ± 0.06	0.023 ± 0.015
10	4	29.4	0.11 ± 0.07	0.033 ± 0.019
12	3	16.9	0.07 ± 0.05	0.029 ± 0.020
14	0	--	--	--
16	1	8.0	$0.03 \, {}^{+0.06}_{-0.02}$	$0.048 \, {}^{+0.097}_{-0.028}$
Total	25	152.0	0.59 ± 0.23	0.028 ± 0.010
Forward*	6	66.4	0.26 ± 0.14	0.012 ± 0.007
Backward	19	85.6	0.33 ± 0.14	0.016 ± 0.007

*For $0<x<0.1$

TABLE V-B

Cross Sections for $\pi^- p \rightarrow \bar{\Lambda}$ + Anything

for $x<0.0$

Number of Charged Particles Produced n_{ch}	Number of Fitted $\bar{\Lambda}$	Weighted Number	$\sigma_{n_{ch}}$ $(\bar{\Lambda})$ mb	$\bar{n}_{\bar{\Lambda}^0}$ per inelastic interaction
2	0	0	$0.06\ ^{+0.06}_{-0.04}$	$0.038\ ^{+0.038}_{-0.025}$
4	2	8.8	0.03 ± 0.02	0.017 ± 0.011
6	7	25.5	0.10 ± 0.04	0.038 ± 0.020
8	4	13.8	0.05 ± 0.03	0.023 ± 0.015
10	4	29.4	0.11 ± 0.07	0.033 ± 0.019
12	2	7.6	0.03 ± 0.03	0.029 ± 0.020
14	0	--	--	--
16	0	0	$0.03\ ^{+0.06}_{-0.02}$	$0.048\ ^{+0.097}_{-0.028}$
Backward	19	85.6	0.33 ± 0.14	0.016 ± 0.007

TABLE VI

Comparison of Backward Neutral Particles Produced Per Inelastic Interaction for 205 GeV/c $\pi^- p$ and pp

Neutral Particle	$\bar{n}_{\pi^- p}$	$\bar{n}_{pp}$[a]
K_S^0 (backward)	0.091 ± 0.011	0.085 ± 0.005
Λ (backward)	0.059 0.010	0.055 ± 0.005
$\bar{\Lambda}$ (backward)	0.016 0.007	0.013 ± 0.004
γ (backward)	3.97 0.3	

[a] Reference 25.

TABLE VII

Λ and $\bar{\Lambda}$ Moments

Moment	Λ with $x < -0.15$	Λ with $-0.15<x<0.3$	$\bar{\Lambda}$ with $x<0.1$
$\langle n_{ch} \rangle$	5.9 ± 0.7	8.8 ± 1.2	7.65 ± 1.2
$\langle n_{ch}^2 \rangle$	45 ± 10	91 ± 17	71 ± 20

TABLE VIII

Multiple Neutral Strange Particle Production

Pair Produced	Pairs Observed	Cross Section (mb)
$K_s^oK_s^o$	7	0.26 ± 0.13
$K_s^o\Lambda$	9	0.21 ± 0.08
$K_s^o\bar{\Lambda}$	1	$0.24 {}^{+0.56}_{-0.20}$
$\Lambda\ \bar{\Lambda}$	3	$0.18 {}^{+0.17}_{-0.10}$

TABLE IX

SINGLE-EXPONENTIAL FIT TO p_T^2 DEPENDENCE OF NEUTRAL PARTICLE

Particle	Slope $(GeV/c)^{-2}$	χ^2	Degrees of Freedom
K_S^0	3.97 ± 0.50	11.5	7
Λ	3.18 ± 0.14	0.2	4
$\bar{\Lambda}$	3.8 ± 1.3	0.7	2

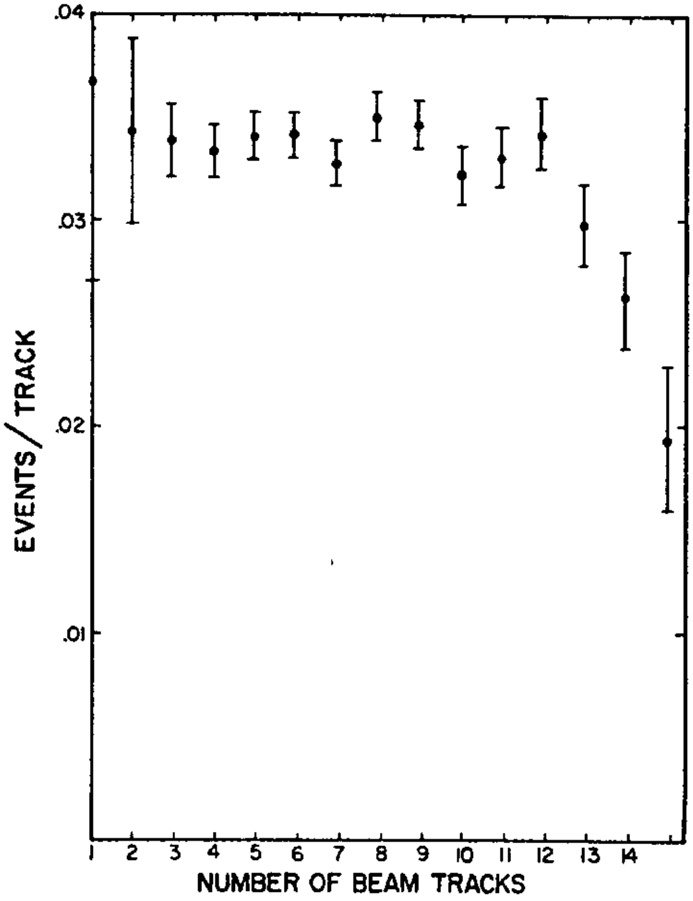

Fig. 1: Scanned events (of all types) per beam track as a function of the number of beam tracks in the frame.

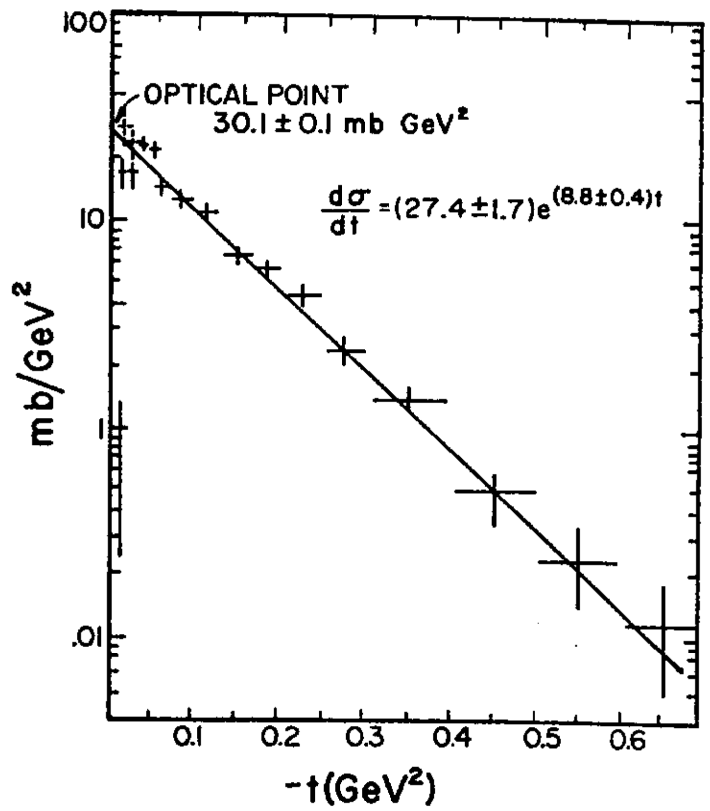

Fig. 2: Elastic differential cross section. For $0.01 < -t < 0.03$ GeV², the solid points represent the observed events, and the dashed points represent the estimated number of events, after correcting for scanning losses (see text). Solid curve is a fit to the form Ae^{-bt} for $0.03 < -t < 0.06$ GeV², yielding $A = 27.4 \pm 1.7$ mb/GeV² and $b = 8.8 \pm 0.4$ GeV^{-2}.

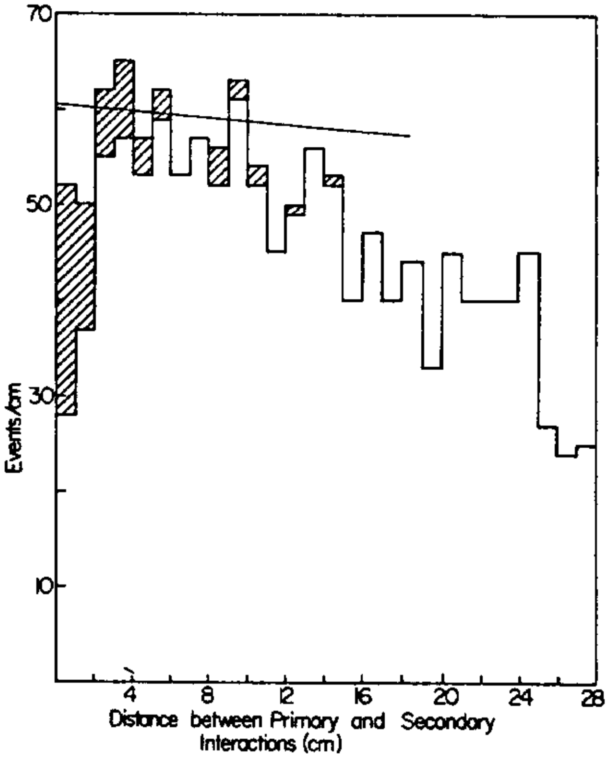

Fig. 3: Distribution of distances on the scan table between primary and secondary interactions. Shaded are events for which the separation of prongs between primary and secondary vertex was impossible. Solid curve is predicted distribution of projected distance to secondary interaction normalized to an expected interaction length of 9.5 m (see text).

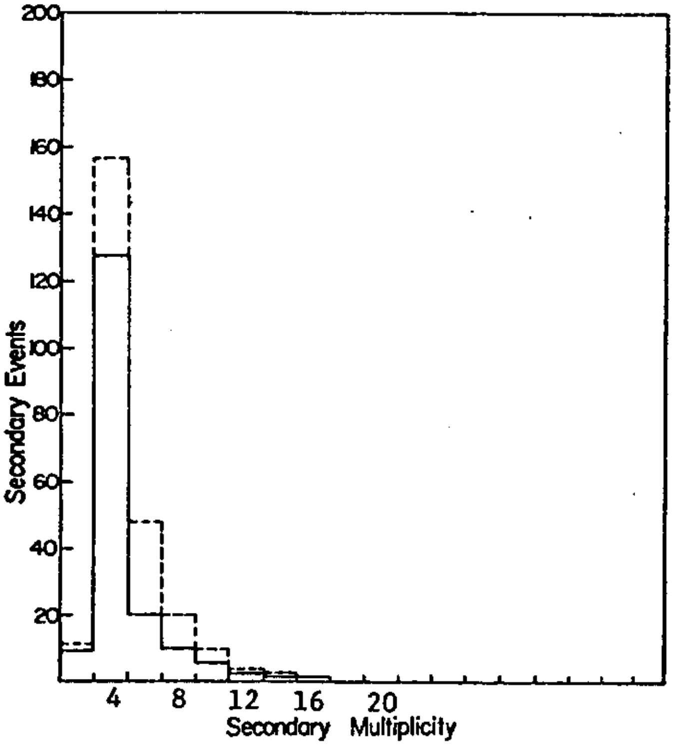

Fig. 4: Prong distribution for secondary events within 4 cm (on the scan table) of the primary vertex. Solid line shows distribution for events resolved by the scanners; dashed line indicates estimated correction for missed or unresolved secondaries, based on those found beyond 4 cm.

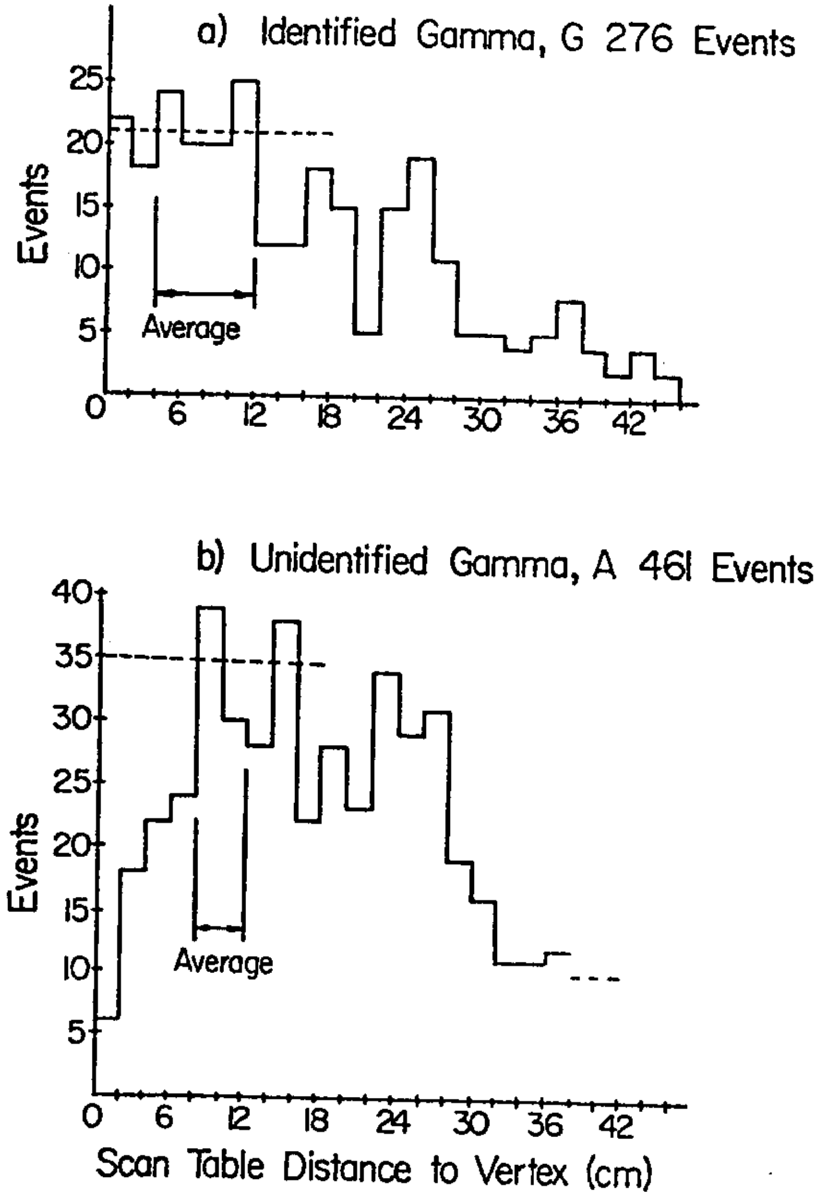

a) Identified Gamma, G 276 Events

b) Unidentified Gamma, A 461 Events

Fig. 5: Distribution of distances on the scan table between primary vertex and gamma vertex. The dashed line indicates the predicted distribution of projected distance to the γ conversion for a conversion length of 12.7 m normalized to the number observed between 4 and 12 cm for identified gamma (G), and between 8 and 12 cm for unidentified gamma (A).

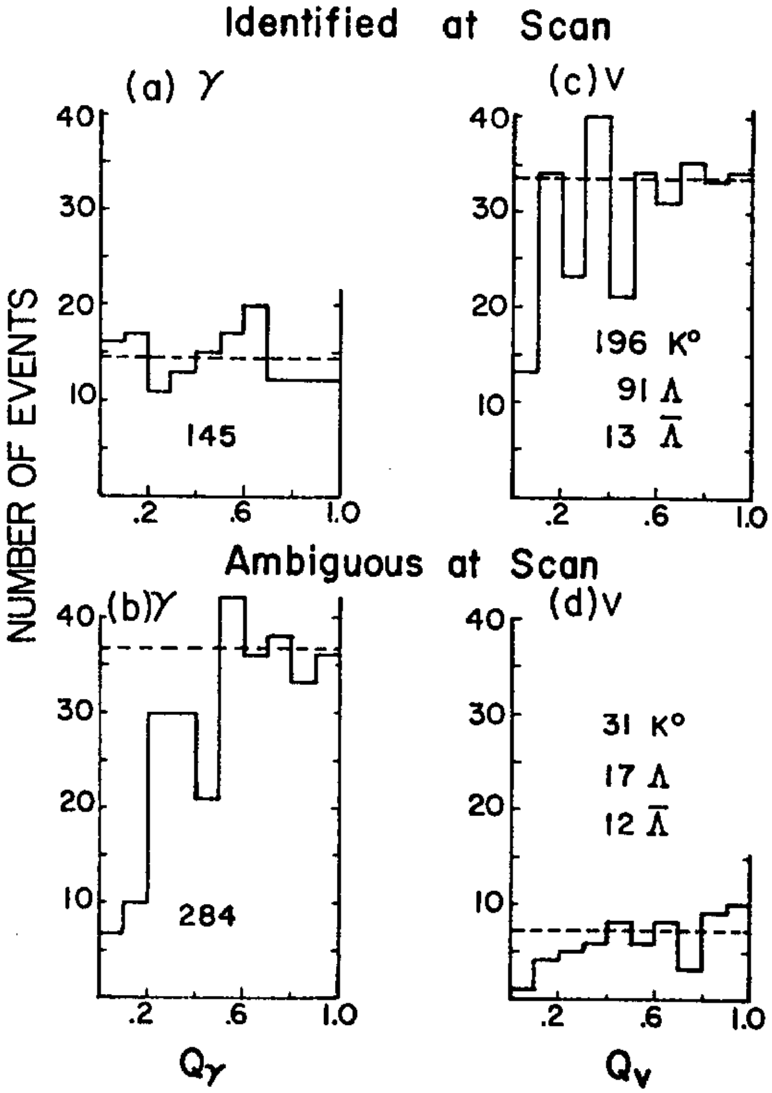

Fig. 6

Fig. 6: Conversion probability distributions for identified (G,V) and unidentified (A) gamma and neutral strange particles. The dashed lines are normalized between 0.5 and 1.0.

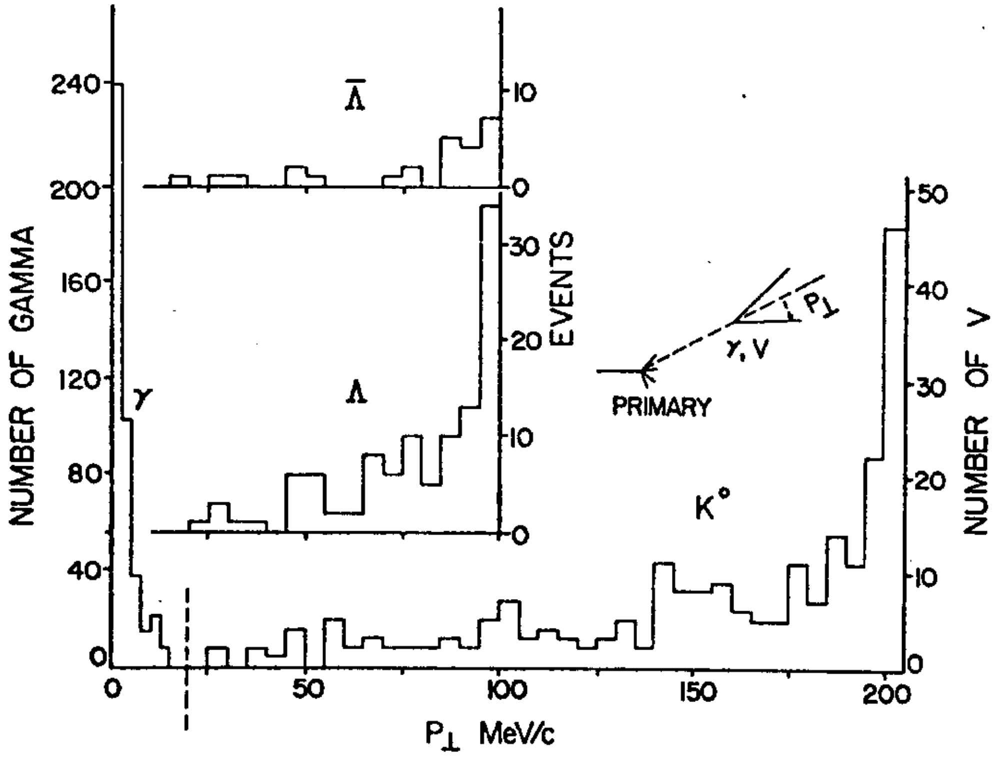

Fig. 7

See text for discussion and definitions.

Fig. 7: Transverse momentum (fitted values) distributions of the outgoing particles from γ, $\bar{\Lambda}$, Λ and K_s^0. For γ this distribution should be zero except for resolution. For $\bar{\Lambda}$, Λ and K_s^0 the distribution should be tan $\frac{p_\perp}{q^2\sqrt{1-p_\perp^2/q^2}}$ q is the maximum decay momentum.

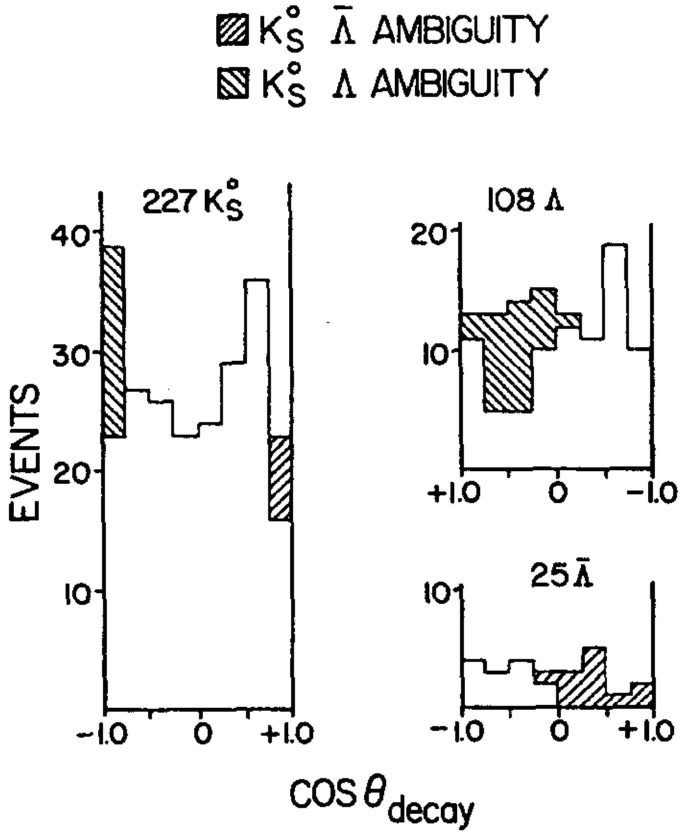

Fig. 8: Cosine of the polar decay angle of the emitted negative in the center of mass of the neutral particle.

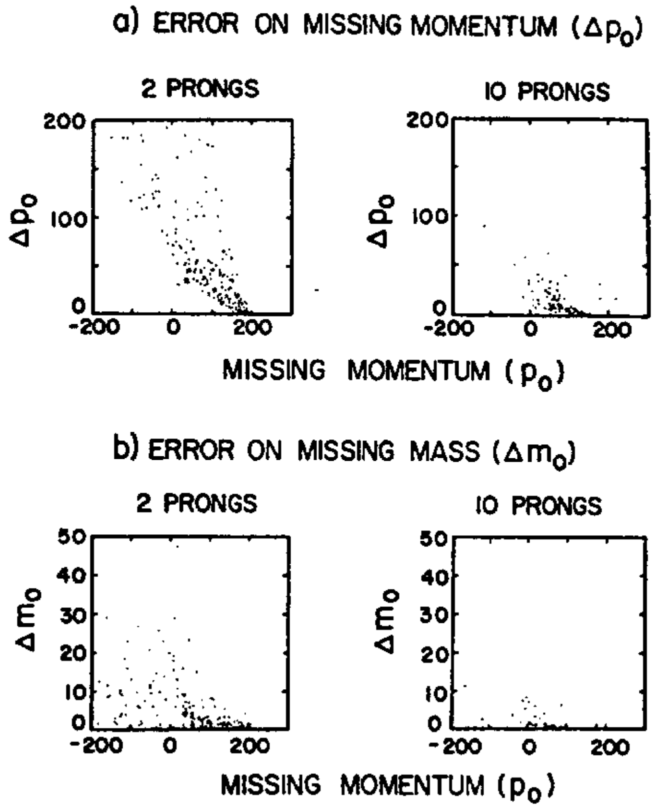

Fig. 9: (a) Error on missing mass as a function of missing momentum. (b) Error on missing momentum as a function of missing momentum. Each is shown for 2 and 10 prongs to illustrate the multiplicity dependence. All events having no missing neutrals, i.e., the four constraint fits have been removed.

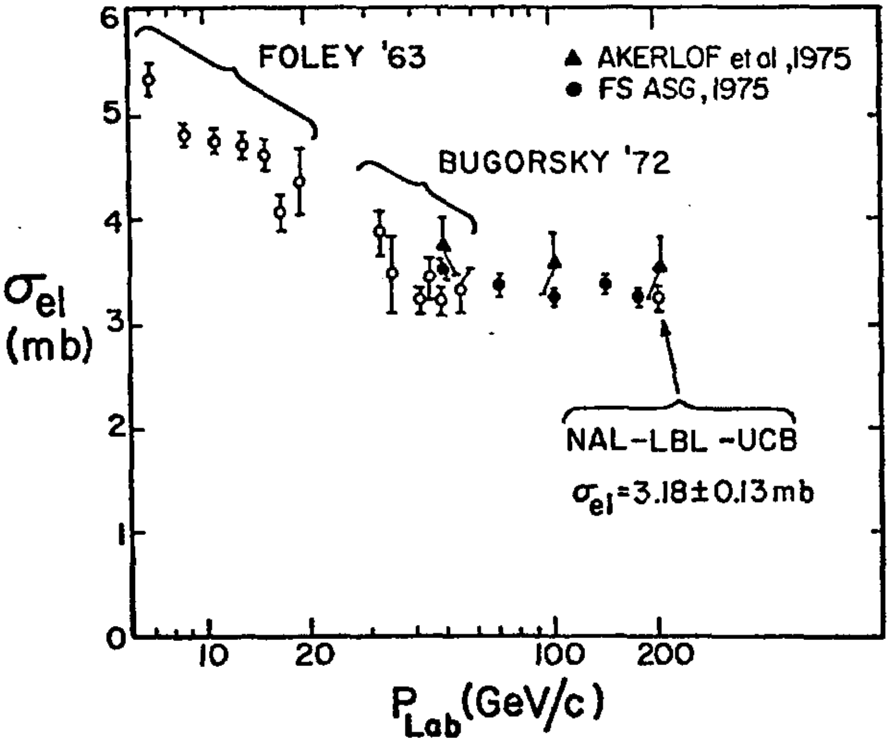

Fig. 10: Elastic cross section for π^-+p as a function of incident π^- momentum.

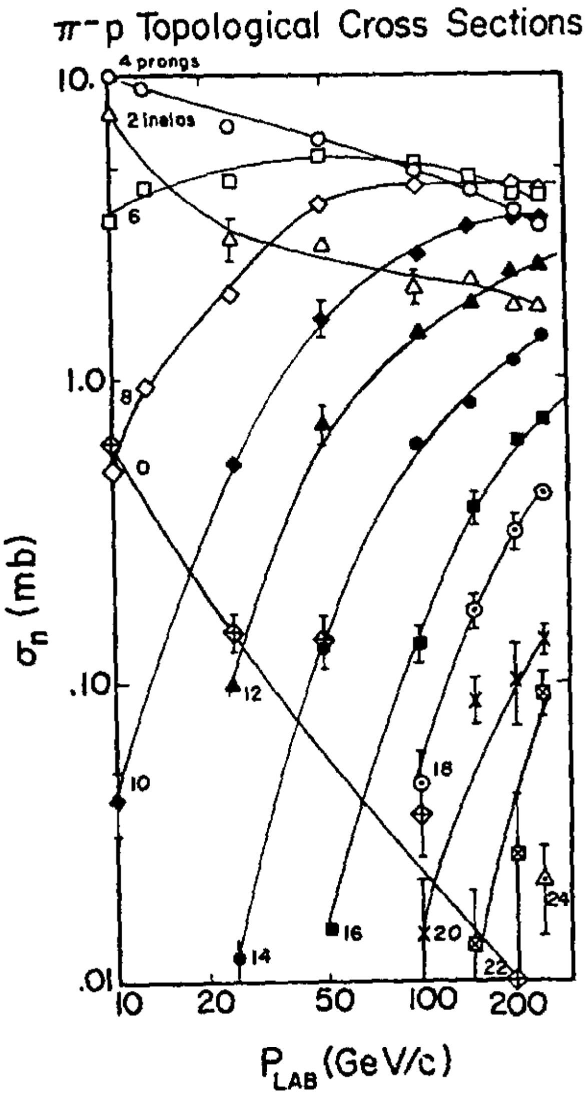

Fig. 11: Topological cross sections for π^-+p as a function of incident π^- momentum.

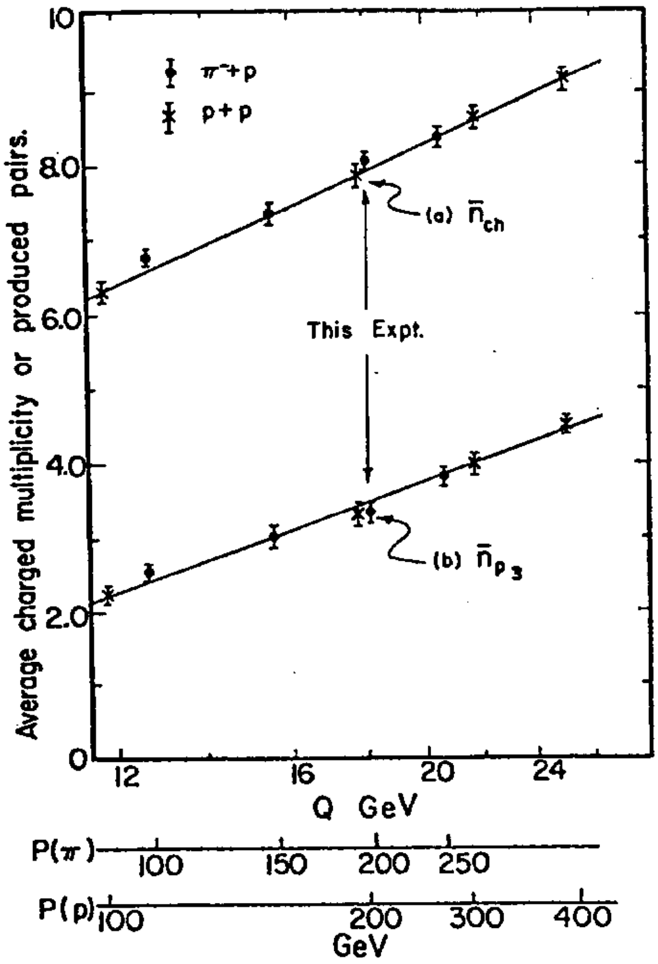

Fig. 12: (a) Average charged multiplicity as a function of Q ($Q = \sqrt{s} - m_{beam} - m_{target}$). (b) Average number of pairs produced as a function of Q. See text for definition of $\bar{n}_p$.

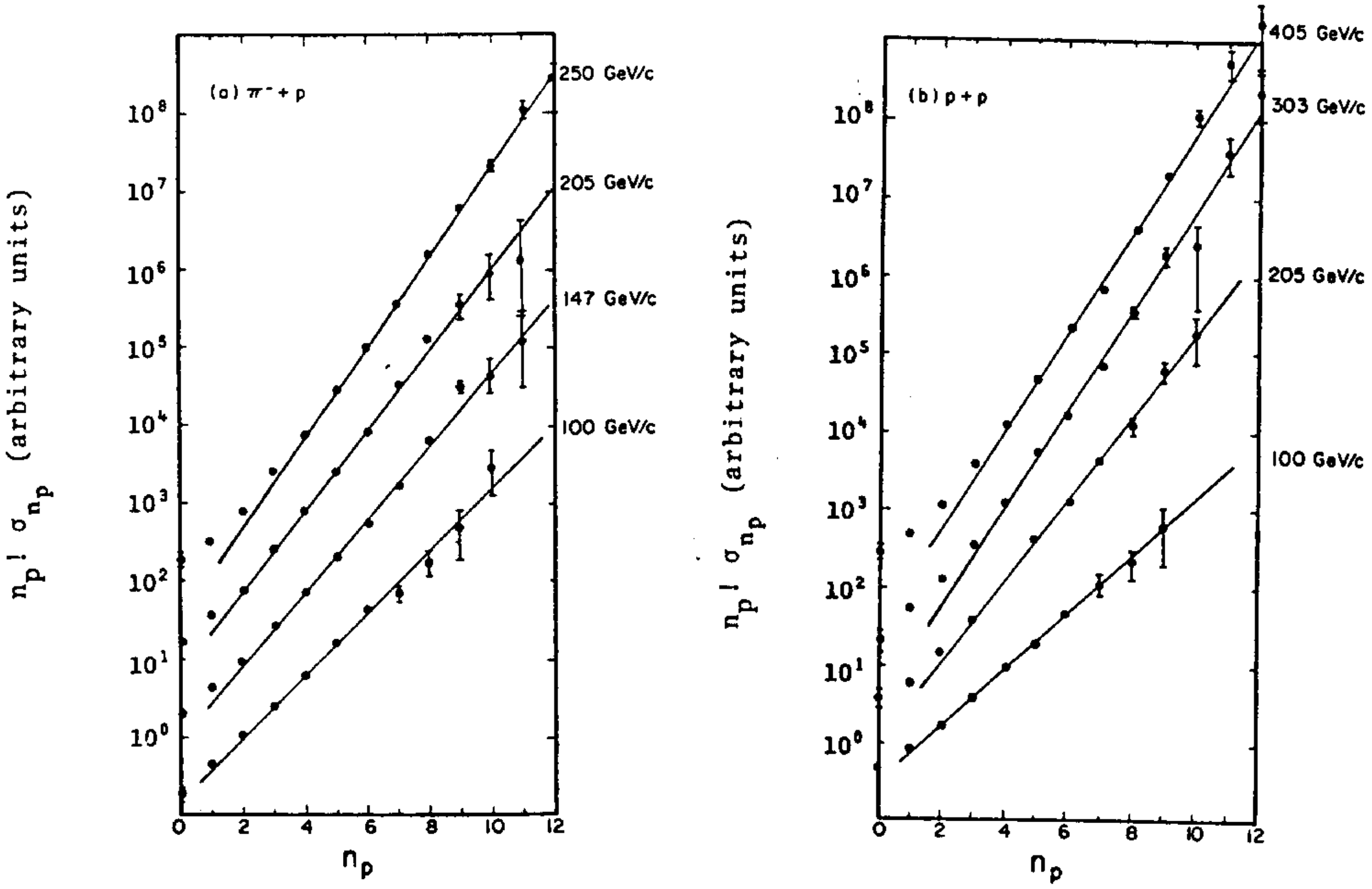

Fig. 13: Plot of $n_p!\sigma_{n_p}$ where $n_p = (n_{ch}/2)-1$ (number of produced pairs). A Poisson distribution would give a straight line. The solid lines are fit to the points for $n_p \geq 3$.

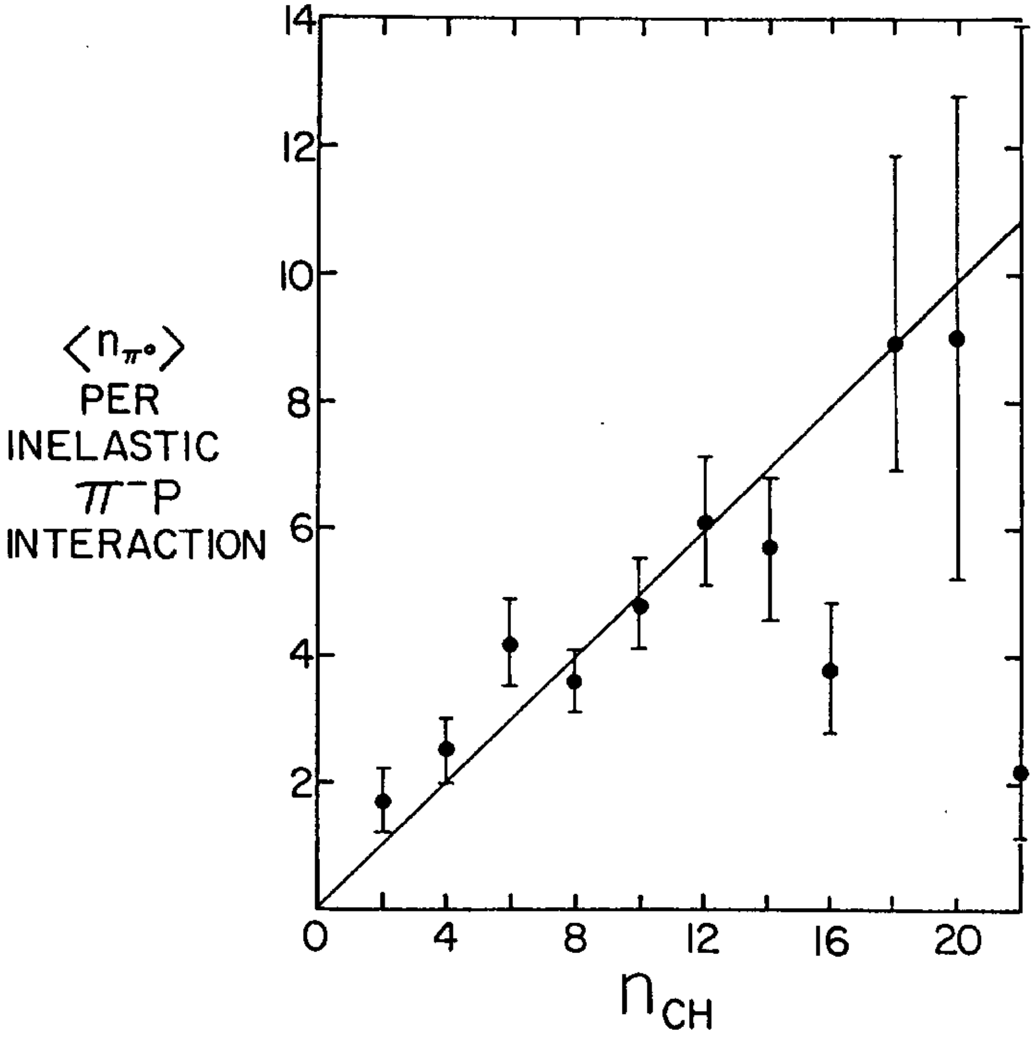

Fig. 14: Average number of π^0 per inelastic interaction as a function of energy. It is assumed that all gamma come from π^0 decay. Straight line in $\langle n_{\pi^o} \rangle = n_{ch}/2$.

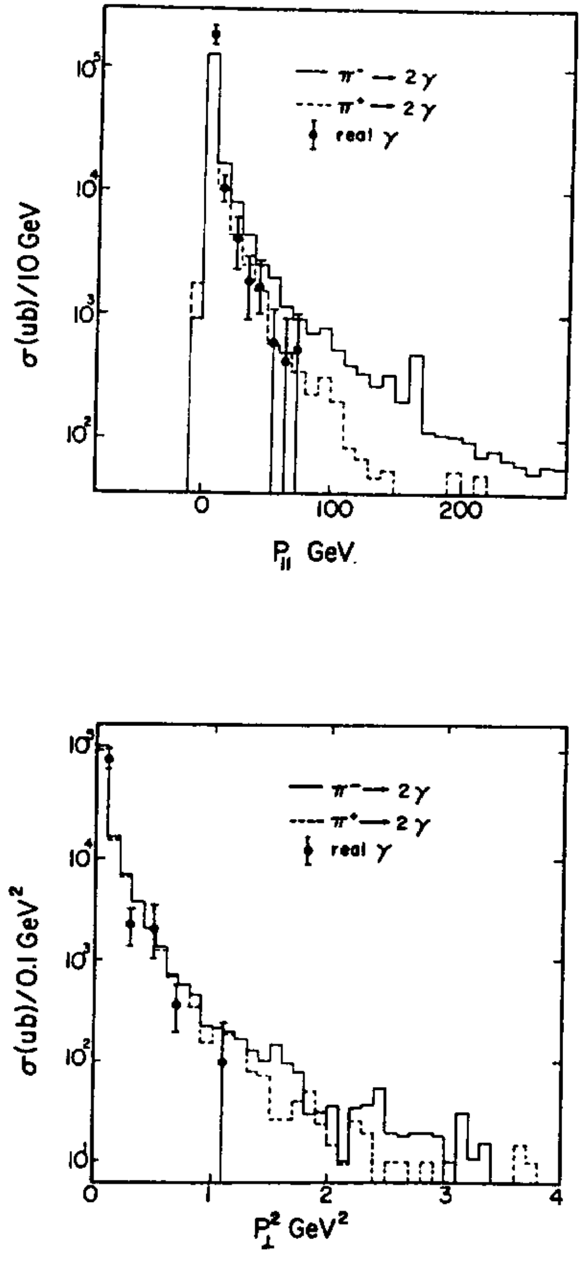

Fig. 15: $P_{||}$ and $p_\perp$ laboratory momentum distributions for observed γ. The solid and dashed curves were generated by letting $\pi^\pm$ "decay" isotropically to 2γ.

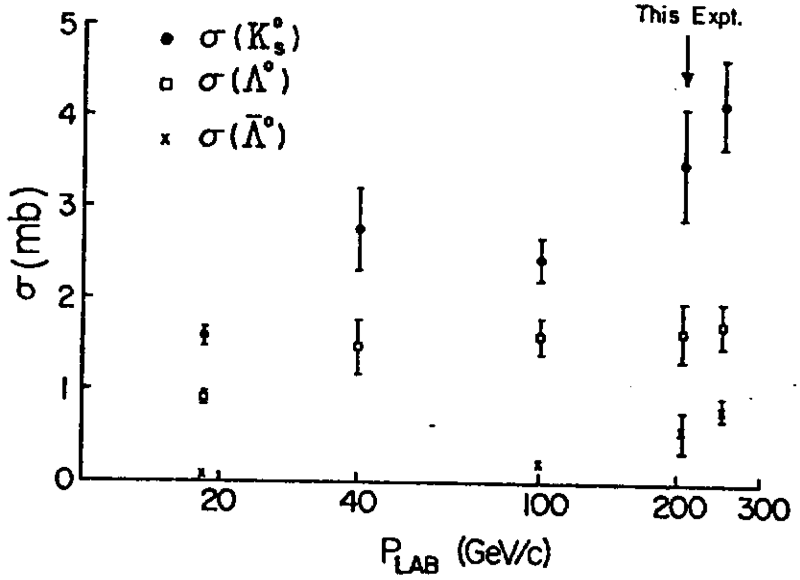

Fig. 16: Neutral strange particle inclusive cross sections as a function of beam momentum for π^-p interactions. Data are from this experiment and References 21-24.

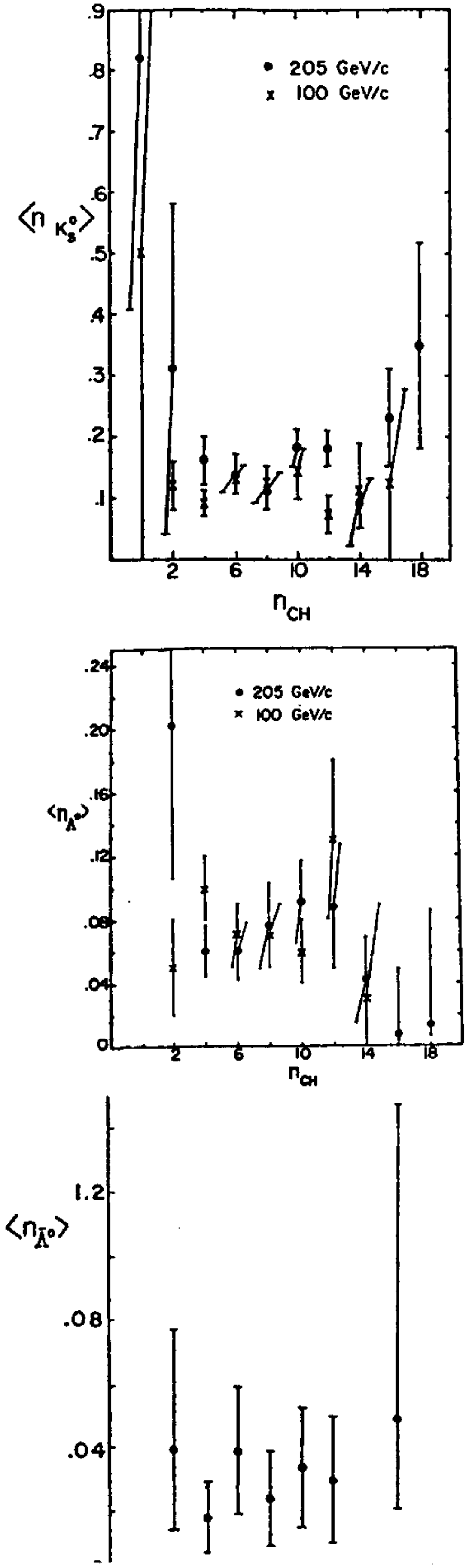

Fig. 17: Average number of Λ, K_S^0 and $\bar{\Lambda}$ per inelastic interaction as a function of the number of charged particles for this

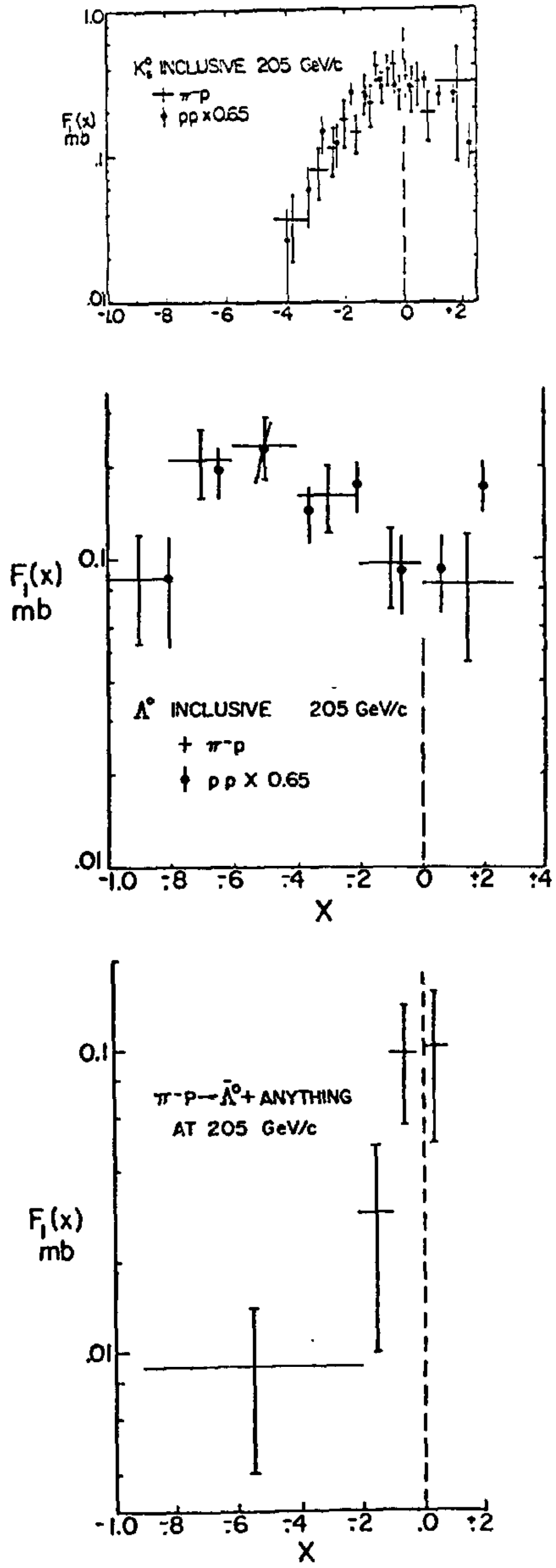

Fig. 18: $F_1(x)$ for Λ, K_s^0 and $\bar{\Lambda}$ production for this experiment and for 205 GeV/c pp (except $\bar{\Lambda}$, Reference 25), normalized to

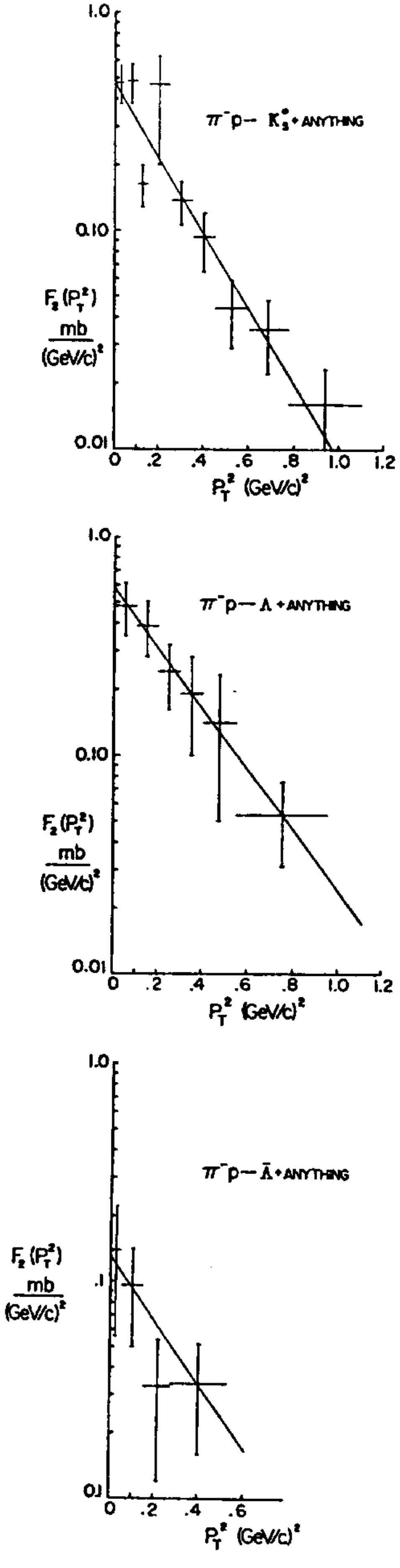

Fig. 19: $F_2(p_T{}^2)$ for Λ, K_S^0 and $\overline{\Lambda}$ production. Solid line represents

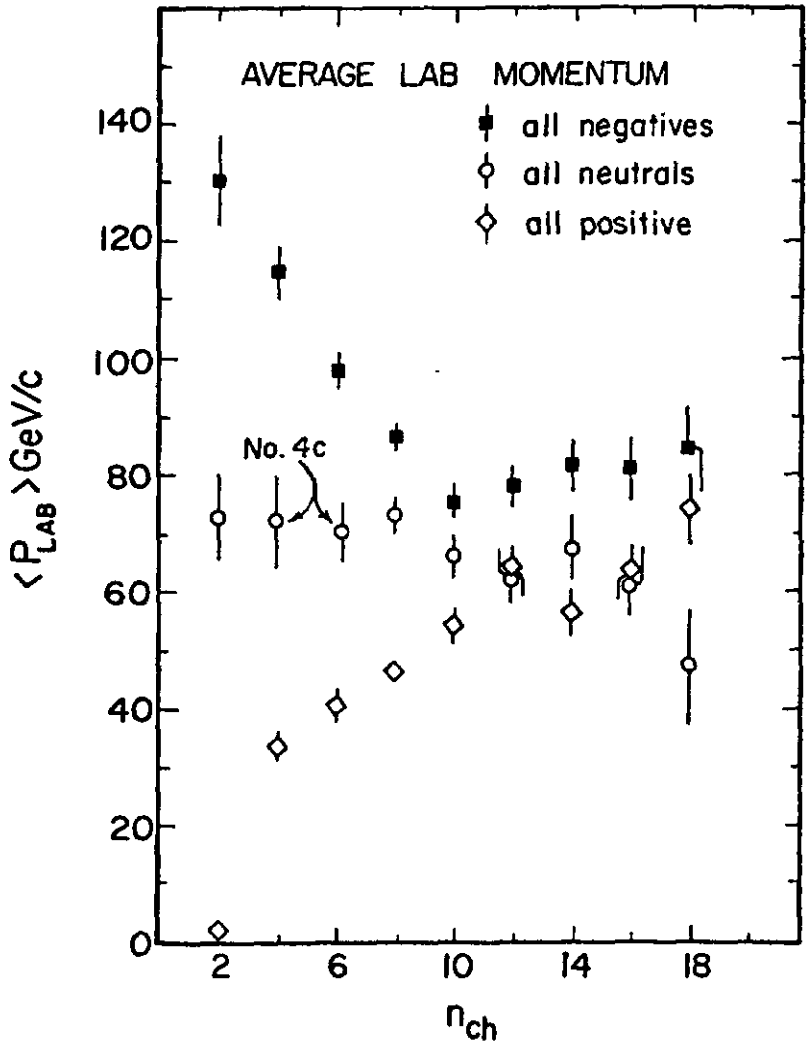

Fig. 20: Average laboratory momentum for the sum of all negatives, neutrals and positives as a function of multiplicity. Events with no missing neutrals (4C fits) have been removed.